**FULL-LENGTH PAPER**

THE PROTEIN SOCIETY    WILEY

# Condensation of the β-cell secretory granule luminal cargoes pro/insulin and ICA512 RESP18 homology domain

Pamela L. Toledo[1,2]    |    Diego S. Vazquez[1,2]    |    Alejo R. Gianotti[1,2]    |
Milagros B. Abate[1,2]    |    Carolin Wegbrod[3,4,5]    |    Juha M. Torkko[3,4,5]    |
Michele Solimena[3,4,5]    |    Mario R. Ermácora[1,2] [ID]

[1]Departamento de Ciencia y Tecnología, Universidad Nacional de Quilmes, Provincia de Buenos Aires, Argentina

[2]Grupo de Biología Estructural y Biotecnología, IMBICE, CONICET, Universidad Nacional de Quilmes, Provincia de Buenos Aires, Argentina

[3]Department of Molecular Diabetology, University Hospital and Faculty of Medicine, TU Dresden, Dresden, Germany

[4]Paul Langerhans Institute Dresden of Helmholtz Munich at the University Hospital and Faculty of Medicine, TU Dresden, Dresden, Germany

[5]German Center for Diabetes Research (DZD e.V.), Neuherberg, Germany

**Correspondence**
Michele Solimena, Molecular Diabetology & Paul Langerhans Institute Dresden of Helmholtz Munich, University Hospital and Faculty of Medicine, TU Dresden, Fetscherstrasse 74, 01307 Dresden, Germany.
Email: michele.solimena@tu-dresden.de

Mario R. Ermácora, Departamento de Ciencia y Tecnología, Universidad Nacional de Quilmes, Roque Sáenz Peña 325, (1876), Bernal, Buenos Aires, Argentina.
Email: ermacora@unq.edu.ar

**Abstract**

ICA512/PTPRN is a receptor tyrosine-like phosphatase implicated in the biogenesis and turnover of the insulin secretory granules (SGs) in pancreatic islet beta cells. Previously we found biophysical evidence that its luminal RESP18 homology domain (RESP18HD) forms a biomolecular condensate and interacts with insulin in vitro at close-to-neutral pH, that is, in conditions resembling those present in the early secretory pathway. Here we provide further evidence for the relevance of these findings by showing that at pH 6.8 RESP18HD interacts also with proinsulin—the physiological insulin precursor found in the early secretory pathway and the major luminal cargo of β-cell nascent SGs. Our light scattering analyses indicate that RESP18HD and proinsulin, but also insulin, populate nanocondensates ranging in size from 15 to 300 nm and 10e2 to 10e6 molecules. Co-condensation of RESP18HD with proinsulin/insulin transforms the initial nanocondensates into microcondensates (size >1 μm). The intrinsic tendency of proinsulin to self-condensate implies that, in the ER, a chaperoning mechanism must arrest its spontaneous intermolecular condensation to allow for proper intramolecular folding. These data further suggest that proinsulin is an early driver of insulin SG biogenesis, in a process in which its co-condensation with RESP18HD participates in their phase separation from other secretory proteins in transit through the same compartments but destined to other routes. Through the cytosolic tail of ICA512, proinsulin co-

Pamela L. Toledo, Diego S. Vazquez, and Alejo R. Gianotti contributed equally to this study.

condensation with RESP18HD may further orchestrate the recruitment of cytosolic factors involved in membrane budding and fission of transport vesicles and nascent SGs.

# 1 | INTRODUCTION

Receptor-type protein-tyrosine phosphatases (RPTPs) are multidomain, transmembrane proteins involved in signaling pathways (Andersen et al., 2001). ICA512 (also known as IA-2, PTP35, or PTPRN) and phogrin (also known as IA-2β, IAR, ICAAR, or PTPRN2) are R8 subtype RPTPs expressed in peptide-secreting endocrine cells and neurons, where they are enriched in the membrane of secretory granules (SGs) and large dense-core vesicles, respectively (Wasmeier and Hutton, 1996; Solimena et al., 1996). Both proteins are involved in the biogenesis and turnover of insulin SGs in pancreatic islet β cells (Dirkx Jr and Solimena, 2012; Rohli et al., 2022; Liu et al., 2021; Omar-Hmeadi and Idevall-Hagren, 2021), and their depletion, either alone or in combination, strongly reduces insulin SG stores (Henquin et al., 2008). ICA512 and phogrin multidomain architecture is complex. They have a large N-terminal luminal segment, a single-pass transmembrane region, and a cytoplasmic segment (Figure 1). One of the domains in the N-terminal segment includes a region similar to Regulated endocrine-specific protein 18 (Resp 18).

Like ICA512 and phogrin, Resp18 is expressed solely in peptide-secreting endocrine cells, and its expression is up-regulated in conditions stimulating SG biogenesis (Zhang et al., 2007). The homologous region of ICA512 and phogrin was named "Resp18 homology domain" (RESP18HD). We identified ICA512 RESP18HD as a potential factor for protein SG luminal cargoes condensation and inhibition of amyloidogenesis acting early in the secretory pathway (Torkko et al., 2015; Sosa et al., 2016; Toledo et al., 2019).

Insulin biosynthesis involves elaborated processing, oxidative folding, and biomolecular condensation across multiple cellular compartments (Liu et al., 2021; Kuliawat and Arvan, 1994; Dodson and Steiner, 1998; Liu et al., 2018; Vasiljević et al., 2020; Vazquez et al., 2022). Insulin precursor, preproinsulin, synthesized in the endoplasmic reticulum (ER), is a single chain consisting from N- to C-terminus of a signal sequence followed by the B chain, the excised C-peptide, and the A chain of insulin. In the ER, after the signal sequence processing, proinsulin
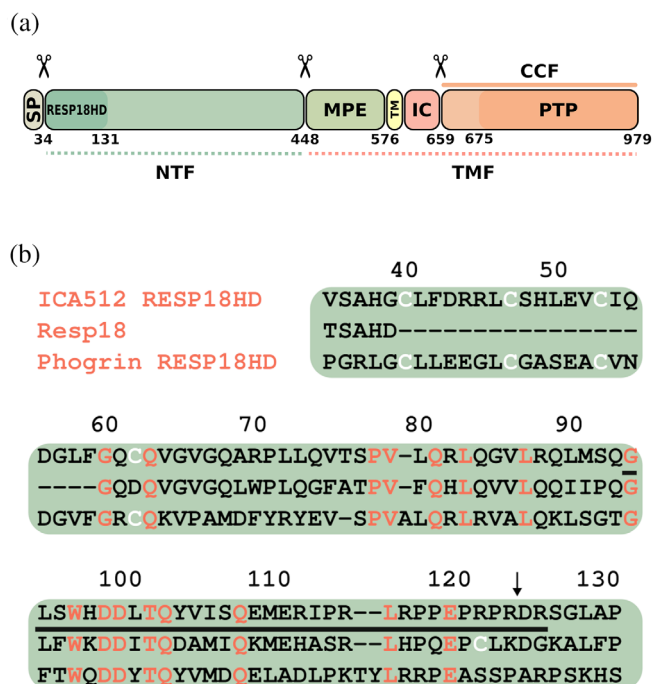


**FIGURE 1** ICA512 domain layout and RESP18HD sequence. (a) The SG luminal segment of ICA512 (UniProtKB Q16849) comprises residues 1–575 and includes a signal peptide (SP), the NTF, and the MPE. The transmembrane domain (TM) comprises residues 576–600. The cytoplasmic region, residues 601–979, is made of the juxtamembrane intracellular domain (IC) and the cytoplasmic cleaved fragment (CCF). Most of the cytoplasmic cleaved fragment corresponds to the pseudo-phosphatase (catalytically inactive) domain (PTP), from which the entire protein is named. Scissors mark characterized processing sites. Convertase-mediated cleavage at residue 448 generates the transmembrane fragment (ICA512 TMF, residues 449–979, corresponding to MPE–TM–IC), which is transiently inserted into the plasma membrane upon exocytosis. ICA512 RESP18HD constitutes the N-terminal portion of ICA512 NTF. (b) Sequence alignment of ICA512 RESP18HD, Resp18 (UniProtKB Q5W5W9), and phogrin RESP18HD (UniProtKB Q92932). Conserved residues and cysteine residues are indicated in orange and white, respectively. An ICA512 RESP18HD C-terminal cleavage site between Arg-124 and Asp-125 in ICA512 RESP18HD is indicated with a down arrow. Most of the IDD accounting for ICA512 RESP18HD condensing activity is the product of exon-4, which encodes for ICA512 residues 94–126 (underlined). IDD, intrinsically disordered domain; MPE, membrane-proximal ectodomain; NTF, N-terminal fragment; SG, secretory granule.

starts to fold, acquires the correct disulfide bonds, and forms non-covalent assemblies (Liu et al., 2018; Haataja et al., 2013). Then, proinsulin and its processing enzymes are transported through the Golgi to the trans-Golgi network (TGN), where it partitions and sorts into immature SGs. The above sequence of events, which is rate limiting for the overall trafficking through the secretory pathway, is captured in the model called "sorting by aggregation" or "sorting for entry" to explain the targeting of insulin to SGs (Liu et al., 2021; Kuliawat and Arvan, 1994; Liu et al., 2018; Haataja et al., 2013; Arvan and Halban, 2004; Dikeakos and Reudelhuber, 2007).

The generation of immature SGs is driven by a complex network of interacting proteins and membranes (Dirkx Jr and Solimena, 2012; Rohli et al., 2022; Liu et al., 2021; Omar-Hmeadi and Idevall-Hagren, 2021; Norris et al., 2021). The depletion of cholesterol, inactivation of cholesterol carriers, and numerous proteins involved in lipid metabolism, regulation, and signaling impact on immature SGs formation (Dirkx Jr and Solimena, 2012; Rohli et al., 2022). Protein kinase D1, ADP-ribosylation factor 1 (ARF1), and Arfaptin-1, which localize to the TGN membrane, also are key players in immature SG budding. Arfaptin-1, which interacts with ARF1, contains a BAR-domain believed to impose or sense curvature on lipid bilayers (Gehart et al., 2012). Brefeldin A-sensitive Arf-GEF inhibits insulin granule biogenesis and insulin secretion (Li et al., 2014). BAR domains form 3D structures that modify the geometry of the membrane, alter its liquid properties, and can promote membrane budding. Other BAR-containing proteins found on immature SGs are ICA69 and its interactor PICK1 (Buffa et al., 2008; Cao et al., 2013), which bind to lipid molecules, mainly phosphoinositides (Simunovic et al., 2019; Holst et al., 2013). The type 2 diabetes gene product STARD10 is a phosphoinositide-binding protein that controls insulin SG biogenesis (Carrat et al., 2020). Similarly, secretogranin III binds cholesterol and associates with the granule membrane, where it anchors chromogranins A (CGA) and secretogranin II. Conspicuous cargoes of SGs, carboxypeptidase E (CPE), chromogranins B (CGB), prohormone convertase 1/3 (PC1/3), prohormone convertase 2 (PC2), also associate to the budding membrane and may impact the membrane topology, although the precise mechanism of this association is still unclear (Rohli et al., 2022 and references therein). In addition, the prohormone neurosecretory protein VGF is necessary to facilitate efficient exit of granule cargo from the TGN and proinsulin processing (Stephens et al., 2017).

SG maturation involves biochemical and biophysical transformations, the most important of which are the conversion to mature insulin by prohormone convertases PC1/3, and PC2 luminal acidification, composition changes, and $Zn^{2+}$ flux mediated insulin hexamerization

and crystallization (Liu et al., 2021; Dikeakos and Reudelhuber, 2007; Paroutis et al., 2004; Lemaire et al., 2009; Suckale and Solimena, 2010; Lisi et al., 2014; Ramazanov et al., 2021). Initially, in the ER lumen, proinsulin is likely to be in a low-aggregation soluble state. In its journey through the Golgi apparatus, the material properties of proinsulin change, becoming a condensate. In the SGs this condensate changes further as proinsulin is progressively converted into insulin and the immature SG into a mature SG, with the condensate being now semicrystalline. After the regulated secretory stimulus, that is, upon elevation of blood glucose levels, the mature SG fuse to the plasma membrane to release insulin into the circulation. In preparation for its hormone function, secreted insulin changes again its condensation state and dissolves in the bloodstream into monomers.

Despite several decades of intensive investigation, many aspects of the SG biogenesis and regulated hormone secretion are incompletely understood. Particularly, the molecular mechanisms underlying the selective sorting of insulin SG cargoes in the pancreatic islet β cells constitute a matter of lively debate (Kuliawat and Arvan, 1994; Arvan and Halban, 2004). The crucial steps in the sorting process occur in the trans-Golgi network (TGN), where the insulin biosynthetic pathway diverge from that of other proteins, either resident in the TGN, or in transit through it, but destined to other routes. A pertinent question is how proinsulin is preferentially enriched in these vesicles. Since no specific receptors have been identified, it is believed that proinsulin is directed to the nascent vesicles by a bulk-flow physical mechanism that somehow separate condensed proteins preferentially from other TGN constituents (Thor et al., 2009). Further sorting into SGs occurs by processes termed "sorting by exit" and "sorting by retention," as small vesicles budding from the SGs selectively remove soluble proteins not destined to the regulated pathway.

Growing evidence indicates that SG cargoes conform a complex, functional, biomolecular condensate (Dikeakos and Reudelhuber, 2007; Ramazanov et al., 2021; Bearrows et al., 2019; Parchure et al., 2022). Common SG residents, such as islet amyloid polypeptide (IAPP), and CGA and CGB have been found to undergo in vivo and/or in vitro conformational transitions that result in biomolecular condensation (Parchure et al., 2022; Zhao et al., 2009; Horvath and Wittung-Stafshede, 2016). Likewise, under a variety of conditions, in vivo and in vitro, insulin forms multimers and nano- and micro-condensates with different material properties: liquid condensation, amorphous aggregation, crystallization, and fibrillation (Dodson and Steiner, 1998; Lemaire et al., 2009; Nielsen et al., 2001; Attri et al., 2010; Wijesekara et al., 2010; Landreh et al., 2012; Xu et al., 2012; Nilsson, 2016; Dzianová et al., 2020; Kaissaratos et al., 2021; Karmakar et al., 2022; Silva-Jr

et al., 2022; Asai et al., 2022). CGB undergoes liquid–liquid phase separation under conditions mimicking those present in the TGN, where proinsulin was found organized as dynamic puncta and co-localized with PC2. Accordingly, CGB and proinsulin co-condensed in vitro (Bearrows et al., 2019; Parchure et al., 2022). In turn, CPE, PC1/3, and PC2 were shown to aggregate and associate with lipid rafts in the granule membrane and might serve as membrane binding sites for cargo condensates (Rohli et al., 2022; Blázquez et al., 2000; Arnaoutova et al., 2003; Assadi et al., 2004; Zhang et al., 2003; Lee and Lindberg, 2008).

The avalanche of studies in recent years underscores the central role of biomolecular condensates in membrane-free subcellular compartmentalization that permits the spatiotemporal organization and regulation of myriads of simultaneous biochemical reactions and macromolecular interactions. These studies have also shown that biomolecular condensation, driven by multivalent intermolecular interactions, is mediated by order–disorder transitions of protein conformation and by protein domain architecture. Conceptually, protein condensation is a distinct level in the protein conformational landscape in which collective folding of large collections of molecules takes place. Biomolecular condensates arise by the physical process of phase separation and comprise a variety of bodies ranging from membrane free organelle-like entities to liquid condensates to solid-like conglomerates. These condensates span a range of lengths from mesoscopic clusters (or nanocondensates) to larger micrometer-sized microcondensed bodies (Vazquez et al., 2022). In a previous work, we reported that ICA512 RESP18HD co-aggregates with insulin (Toledo et al., 2019). Here, we studied in more detail biochemical and biophysical aspects of the in vitro co-condensation of RESP18HD, insulin, and proinsulin and found more evidence in support of their hypothesized physiological significance in SG biogenesis.

## 2 | RESULTS

### 2.1 | Definitions and clarifications

In this work, we use the term "condensate" to describe the nonstoichiometric and non-covalent assembly of protein molecules. This definition makes no assumption about the material properties of the condensates. In the same sense, we define "condensation" as the process by which the condensates form. In previous works, we reported the insulin-condensing activity of RESP18HD131 (Toledo et al., 2019). Here, we study the condensing activity of a seven-residue-shorter variant, RESP18HD124, not only toward insulin, but also proinsulin. We focus on RESP18HD124 because it has better solubility than RESP18HD131 and was identified as a potential product of the stimulated secretion-coupled processing of ICA512 in cells (Toledo et al., 2019). On the other hand, the insulin-precursor proinsulin is a main focus of this study, since its condensation in the TGN may be important for the assembly and budding of immature SGs (Parchure et al., 2022).

### 2.2 | Co-condensation of RESP18HD124 with insulin or proinsulin monitored by SDS-PAGE

Typically, the condensation reaction of RESP18HD124 with insulin or proinsulin was conducted incubating or co-incubating 2 μM RESP18HD124 and 8 μM insulin/proinsulin at pH 6.8 (see Section 4). Pellets and supernatants isolated from the incubates by centrifugation were analyzed by SDS-PAGE. Insulin or proinsulin incubated in the absence of RESP18HD124 were recovered exclusively from the supernatants (Figure 2, lanes 5, 6, 9, and 10), which suggests that insulin and proinsulin were free of readily sedimentable condensates
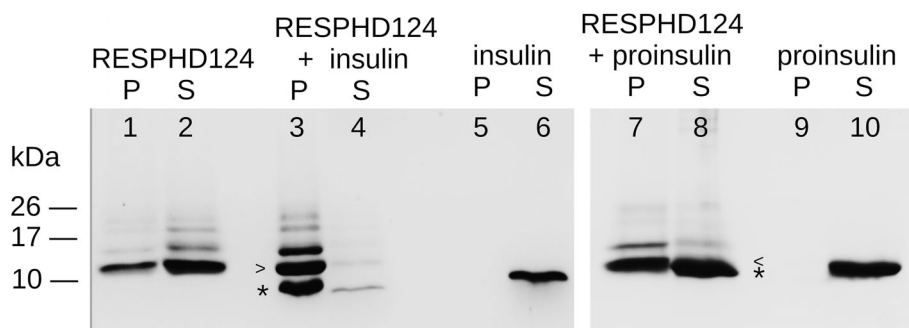


**FIGURE 2** Co-condensation of RESP18HD124 and insulin/proinsulin monitored by SDS–PAGE and Coomassie-blue staining. Proteins were incubated or co-incubated at 20°C and pH 6.8. Pellets (P) and supernatants (S) separated by centrifugation from the incubates were TCA-precipitated and quantitatively loaded into the SDS–PAGE lanes. Arrowheads and asterisks indicate the electrophoretic mobility of RESP18HD124 and insulin/proinsulin, respectively.

(10,000 × g cut-off). Contrastingly, RESP18HD124 incubated alone appeared in both fractions but mainly in the supernatant (Figure 2, lanes 1 and 2), which suggests that it consisted of a mixture of sedimentable and nonsedimentable condensates. In addition to the expected 10.2 kDa band corresponding to RESP18HD124, the gels showed the presence of weak bands in the 15–30 kDa range. These bands were assigned to products of degradative oligomerization of RESP18HD124, which, as reported before, accumulate during incubation and resist the reduction performed in the preparation of the SDS-PAGE samples (Toledo et al., 2019). When co-incubated, RESP18HD124 and insulin localized almost quantitatively to the pellet (Figure 2, lanes 3 and 4). In contrast, in co-incubates of RESP18HD124 and proinsulin, the first localized predominantly in the pellet and the second localized largely in the supernatant (Figure 2, lanes 7 and 8). Since the electrophoretic mobility of RESP18HD124 and proinsulin were similar, their resolution was difficult. However, HPLC analysis of the incubated confirmed that about 10% of the proinsulin localized in the pellet along with RESP18HD124 (Figure S1). All together, these co-incubation experiments suggest that RESP18HD124 possesses a strong condensing activity toward insulin and that this activity is weaker toward proinsulin. In addition, these experiments confirmed and extended our previous reports on the condensing activity of RESP18HD131 and RESP18HD90 (see Figure S2 and Toledo et al., 2019).

## 2.3 | Co-condensation of RESP18HD124 with insulin or proinsulin monitored by scattered light

The co-condensation of RESP18HD with insulin and proinsulin at 20°C and pH 6.8 was additionally shown by an increment of scattered light, which facilitated assessment of the reaction by monitoring the apparent absorbance of the samples (Figure 3). When insulin and proinsulin were incubated alone, these did not condense in the time frame of the assay, while RESP18HD124 showed a slow self-condensation. In contrast, co-incubation of RESP18HD124 with either insulin or proinsulin considerably accelerated condensation. These results showed that RESP18HD124 behaves similarly to RESP18HD131 in the co-condensation with insulin (Toledo et al., 2019) and that, in addition, co-condensates with proinsulin. These co-condensation experiments were conducted also at 37°C. The rate of the reaction increased with temperature, but otherwise the overall result was similar (data not shown).
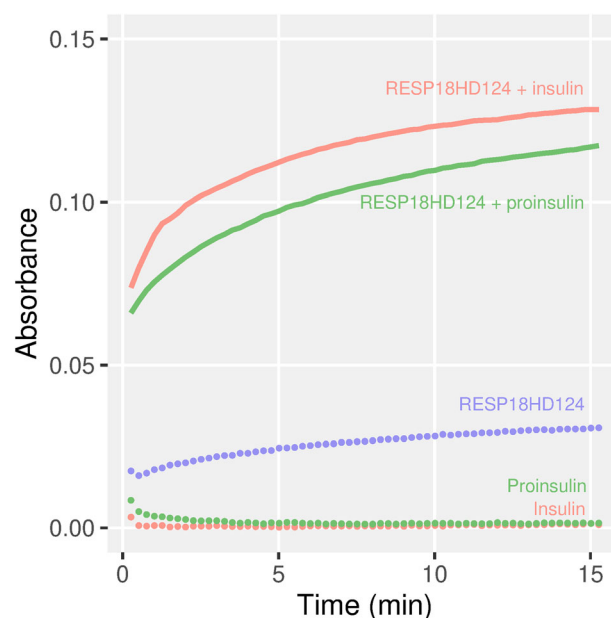


**FIGURE 3** Co-condensation of RESP18HD124 with insulin or proinsulin. The reaction was monitored by light scattering (apparent absorbance at 400 nm). RESP18HD124 (2 μM), insulin (8 μM), and proinsulin (8 μM) were incubated or co-incubated at 20°C and pH 6.8. Averages of three independent experiments are shown.

## 2.4 | Dithiothreitol-driven condensing activity of RESP18HD124

We hypothesized that the conformational destabilization of insulin and proinsulin would accelerate the co-condensation with RESP18HD124. Dithiothreitol (DTT) is a convenient reagent to test this hypothesis because it destabilizes insulin and proinsulin by reducing their disulfide bridges. Indeed, DTT-driven condensation has been used before to characterize the insulin thiol-disulfide exchanging activity of thioredoxin (Holmgren, 1979; Heuck and Wolosiuk, 1997; Yokochi et al., 2019), to evaluate the chaperoning activity of αβ crystallin on insulin and lysozyme (Ghahramani et al., 2020), and in several other studies. Therefore, we modified our reaction protocol including a larger excess of insulin or proinsulin (100 μM) over RESP18HD124 (8 μM) and 1 mM DTT.

The co-condensing activity of RESP18HD124 under the conditions of the modified assay in the time of the experiment is shown in Figure 4. The scattered light from insulin and proinsulin samples was negligible and constant, which indicates that 1 mM DTT does not induce significant condensation of these molecules in the absence of RESP18HD124. When incubated alone, with and without DTT, RESP18HD124 displayed similar, low-amplitude saturation curves. This indicates that the pH shift from 4.5
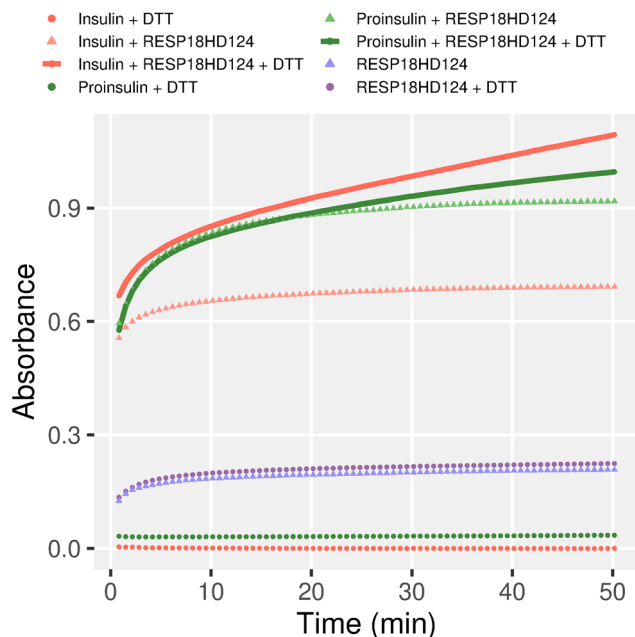
**FIGURE 4** DTT driven co-condensation of insulin and proinsulin. The reaction protocol of Figure 3 was modified as to include a large excess of insulin or proinsulin (100 μM) over RESP18HD (8 μM) and 1 mM DTT in the reaction medium. Averages of three independent experiments are shown. DTT, dithiothreitol.

**FIGURE 5** DTT-driven condensation of insulin and RESP18HD-NEM. RESP18HD124-NEM is a variant of RESP18HD124 fully S-alkylated with N-ethylmaleimide. The reaction conditions were the same as in Figure 4. The well-known reaction between insulin, TRX, and DTT was included as a control (see the main text). Averages of three independent experiments are shown. DTT, dithiothreitol; TRX, thioredoxin.

(RESP18HD124 storage condition) to 6.8 (condensation assay condition) is sufficient to induce a change in the aggregation status of RESP18HD124. When co-incubated with RESP18HD124 in the absence of DTT, insulin and proinsulin displayed saturation curves with large amplitudes and were close to completion in the dead time of mixing. In the presence of DTT, co-incubates of RESP18HD124 with insulin or proinsulin displayed reaction curves that at short times were similar to those in the absence of DTT, but at longer times increased continuously without reaching a plateau. Altogether the above results suggest that RESP18HD124 is a potent inducer of the co-condensation reaction for both insulin and proinsulin, and that this activity does not depend on the redox status of the reactants. However, the reaction course in the presence of DTT suggests that the reduced reactants are better substrates for co-condensation.

The free thiols of RESP18HD are highly reactive and participate in thiol-disulfide exchange reactions (Sosa et al., 2016), and therefore we suspected that they might have a thioredoxin-like, thiol-disulfide oxidoreductase activity accompanied by insulin/proinsulin aggregation and light scattering increase (Holmgren, 1979) (Figure 5; Boxes S1 and S2). To test whether a thiol-disulfide exchange reaction involving RESP18HD cysteine residues have an impact in the co-condensation with insulin/
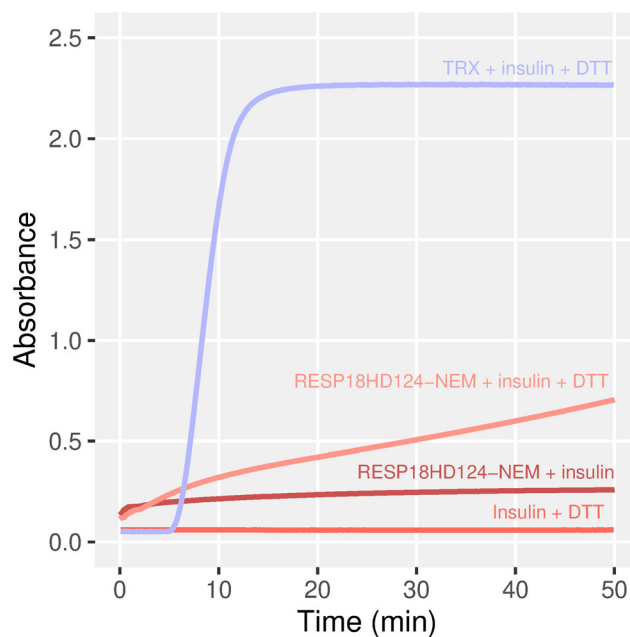
proinsulin we prepared several cysteine point mutants. However, the negative effect of the mutations on the expression and solubility of RESP18HD made it impossible to carry out the co-condensation assays. Instead, we performed the reaction with RESP18HD124–NEM, a variant of RESP18HD124 fully S-alkylated with N-ethylmaleimide. As shown in Figure 5, RESP18HD124–NEM in the presence of DTT induced the co-condensation of insulin. However, the reaction was slower and of less amplitude than that of unmodified RESP18HD124. This result confirms that the presence of free thiol groups is not essential for the co-condensing activity of RESP18HD124. An explanation for the kinetic difference could be that blocking the thiol groups of RESP18HD124 with NEM causes a conformational change that slowed the rate of the co-condensation reaction.

## 2.5 | The co-condensation of RESP18HD124 with insulin or proinsulin involves nanocondensates

Protein nanocondensates—also named mesoscopic clusters—are metastable bodies typically with sizes up to a few hundred of nanometers and $10^3$–$10^6$ molecules

(Vazquez et al., 2022). Nanocondensates are deemed important precursors in nucleation processes, such as aggregation, liquid–liquid phase separation, fibrillation, and crystallization, that characterize many physiological and pathological conditions (Choi et al., 2020; Wühr et al., 2022). Nanocondensates of insulin have been observed before (Xu et al., 2012; Kaissaratos et al., 2021; Orci et al., 1987), and we previously reported the formation of nanocondensates of RESP18HD131 (Sosa et al., 2016; Toledo et al., 2019).

DLS analysis of RESP18HD124 stock solutions at pH 4.5 (Figures 6 and S3) revealed a broad intensity
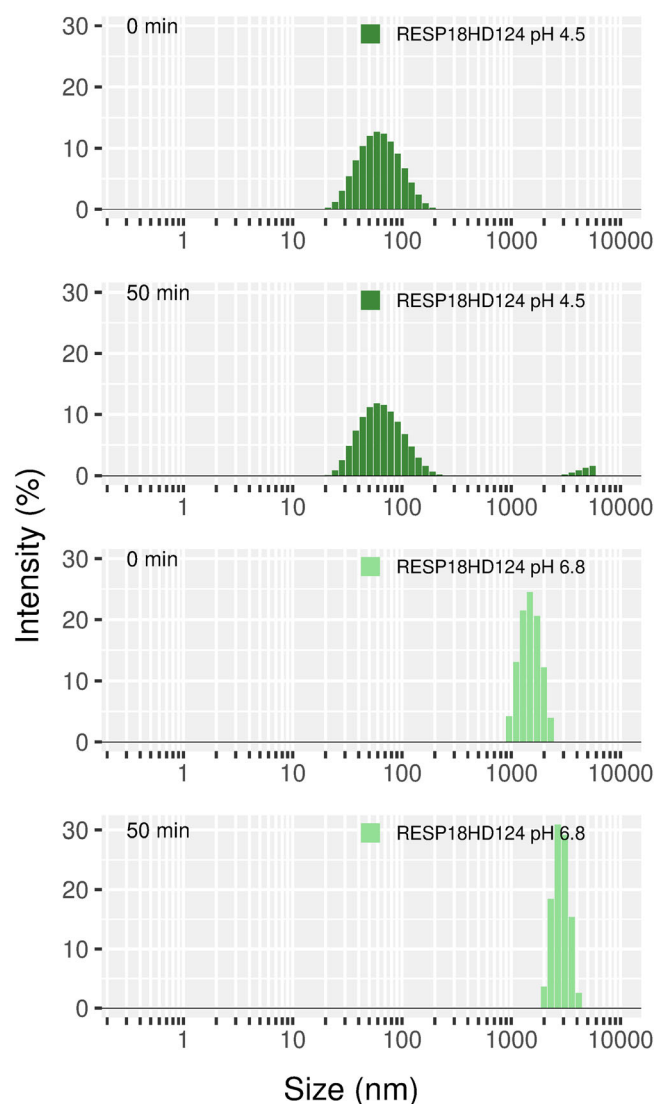


**FIGURE 6** DLS size distribution of RESP18HD124. Measurements at pH 4.5 correspond to the condition of RESP18HD124 storage. Measurements at pH 6.8 correspond to the condensation assay condition and incubation times of Figure 3. Twelve or more replicates for each sample were automatically processed by the Zetasizer's software. Averages of two or more, independent experiments are shown.

distribution peak compatible with an average particle size of 60 nm in diameter, which remained essentially unchanged after a 50-min incubation with or without DTT. Based on particle diameter, molecular mass, specific volume, and assumed volume fraction, we conclude that at pH 4.5, and before the co-condensation reactions, RESP18HD124 populates a nanocondensate of roughly $3 \times 10^3$ molecules. Upon dilution into the initial condensation assay conditions, that is, pH 6.8 and without DTT, the DLS analysis of RESP18HD124 evidenced an average particle of $\sim$1500 nm in diameter ($4 \times 10^7$ molecules), which increased to $\sim$3000 nm ($4 \times 10^8$ molecules) after a 50-min incubation (Figure 6). With the addition of DTT, at pH 6.8, the average particle diameters of RESP18HD124 at time zero and 50 min were $\sim$1000 and 1500 nm ($1 \times 10^7$ and $4 \times 10^7$ molecules), respectively (Figure S3).

Insulin incubated at pH 6.8, with or without DTT, exhibited a DLS profile consistent with monomeric, oligomeric, and nanocondensate insulin (Figures 7 and S4). The size distribution was in general agreement with previous measurements in the literature (Xu et al., 2012; Kaissaratos et al., 2021; Silva-Jr et al., 2022). However, in our analysis, the 2 nm peak corresponding to the monomeric fraction was overshadowed by buffer components. It is to be noted that without DTT the nanocondensates of insulin were 100–300 nm in diameter ($2 \times 10^4$–$6 \times 10^5$ molecules) at the beginning of the incubation and decreased to 15–60 nm ($10^2$–$4 \times 10^3$ molecules) after 50 min (Figure 7). With DTT, nanocondensates of insulin were initially larger (100–500 nm), but also decreased in size after the incubation (60–300 nm) (Figure S4). The effect of DTT on the size of the condensates likely reflects conformational changes underwent by insulin upon partial reduction of its disulfide bridges.

The initial size distribution of co-incubates of insulin and RESP18HD124 at pH 6.8 without DTT evidenced broadly-distributed DLS peaks in the range of 600–5000 nm. After a 50 min incubation the initial distribution collapsed to two narrow peaks centered at 800 and 2000 nm (Figure 7). The cognate experiment in the presence of DTT evidenced initial and final monomodal distributions centered at 1500 nm (Figure S4). Importantly, the DLS peaks corresponding to those of insulin incubated alone were undetected in the co-incubates of insulin and RESP18HD124. Although the possibility that the co-incubation may have resulted in similarly-sized but separate nanocondensates of RESP18HD124 and insulin cannot be excluded, we favor a simpler explanation, posing that co-incubation promoted the formation of hetero nanocondensates including both proteins in the same particle. In addition, the increment in size of the nanocondensates upon co-incubation of insulin and RESP18HD124 provided an explanation for the
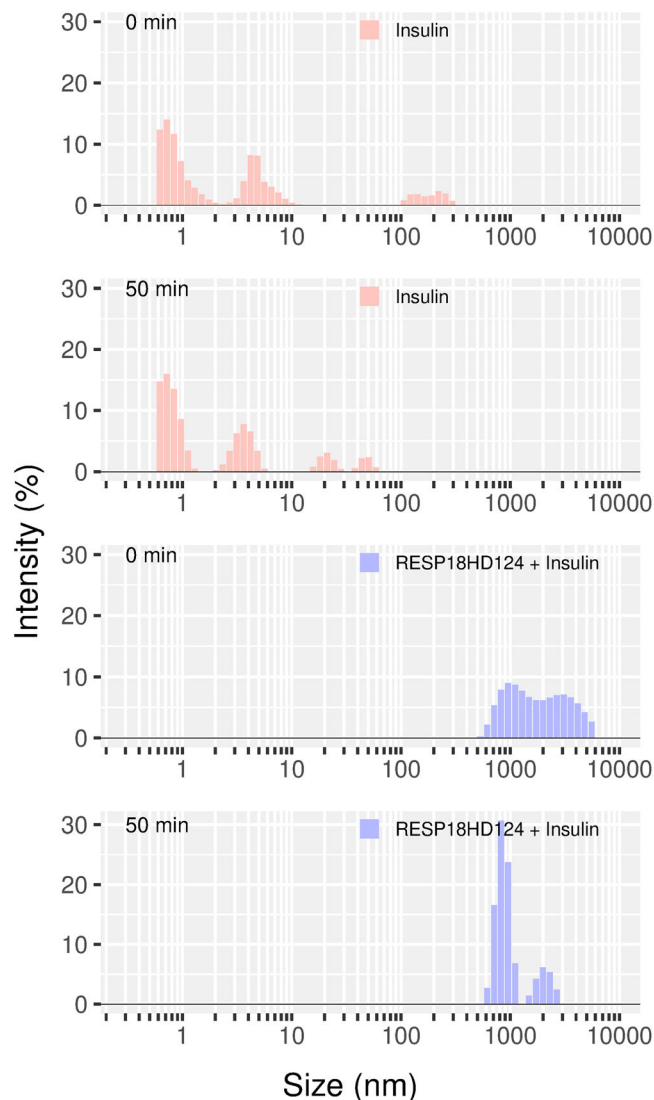
**FIGURE 7** DLS analysis of insulin and co-incubates of RESP18HD124 and insulin. Samples were incubated at pH 6.8, the condensation assay condition. Twelve or more replicates for each sample were automatically processed by the Zetasizer's software. Averages of two or more, independent experiments are shown. DLS, dynamic light scattering.

increment of scattered light that facilitated assessment of the reaction by monitoring the apparent absorbance of the samples (Figures 3 and 4). Indeed, the size of the co-condensates resulting from the co-incubation reaction is more characteristic of typical microscopic aggregates than of nanocondensates.

Proinsulin, incubated alone at the initial and final conditions of the condensation assay, and with or without DTT, exhibited size distributions similar to those of insulin (Figures 8 and S5). The behavior of proinsulin co-incubates with RESP18HD124 was also similar to that of insulin. Without DTT, a single broad peak ranging 600–3000 nm ($3 \times 10^6$–$3 \times 10^8$ molecules) was detected,

which narrowed to 1000–2000 nm ($1 \times 10^7$–$1 \times 10^8$ molecules) after the 50 min incubation (Figure 8). In the presence of DTT and at the time of mixing, the distribution was broader and larger (400–5000 nm; $9 \times 10^5$–$1 \times 10^9$ molecules; Figure S5). Like in the case of the insulin co-aggregation, the peaks corresponding to those of proinsulin incubated alone were absent in the co-incubates with RESP18HD124, which we interpret as an indication that a substantial fraction of proinsulin is included in the co-condensates. Taken together, the DLS and SDS–PAGE results of co-incubation of RESP18HD124 with proinsulin or insulin suggest that these molecules interact in physiologically relevant solution conditions. Such interaction involves nanocondensates that evolve into larger microscopic aggregates.

The biogenesis of SGs starts in the ER with the synthesis of proinsulin, progresses through the Golgi apparatus, and ends with mature SGs scattered throughout the cytoplasm. In the journey, the luminal pH of these subcellular compartments decreases from the close-to-neutral values in the ER and the cis-Golgi, to more acidic in the TGN and finally to 5.5 in the mature SG. Also, $Ca^{2+}$ and $Zn^{2+}$ concentrations change in opposite ways along these compartments (Paroutis et al., 2004; Dzianová et al., 2020; Orci et al., 1987; Kambe et al., 2021). To assess the effects of pH, and $Ca^{2+}$ and $Zn^{2+}$ concentrations, the DLS measurements were performed at pH 7.3, 6.3, and 5.4, and with or without 100 μM $Zn^{2+}$ or 100 μM $Ca^{2+}$ (Figures 9 and 10). The results were similar to those reported above for pH 6.8, suggesting that proinsulin intrinsic tendency to form nanocondensates is not significantly altered by the pH and $Zn^{2+}$ or $Ca^{2+}$ changes along the pathway leading to the mature SG. However, the population of nanocondensates was significantly higher at pH 5.4, with and without the cations, suggesting that in the mature granule the formation of proinsulin nanocondensates is exacerbated.

## 2.6 | Sequence, conformation, and condensation propensity

To get additional insight into the mechanism of the observed co-condensation phenomena, we scrutinized six current phase-separation databases (see Section 4) searching for information on human pro/insulin, and ICA512/IA-2/PTPRN. We found no report of condensing properties for these proteins.

Conformational disorder is a strong determinant of protein condensation, and most protein engaging in it contain intrinsically disordered domains (IDDs) (Vazquez et al., 2022). The NMR proinsulin structure and the AlphaFold model of RESP18HD exhibit regions that
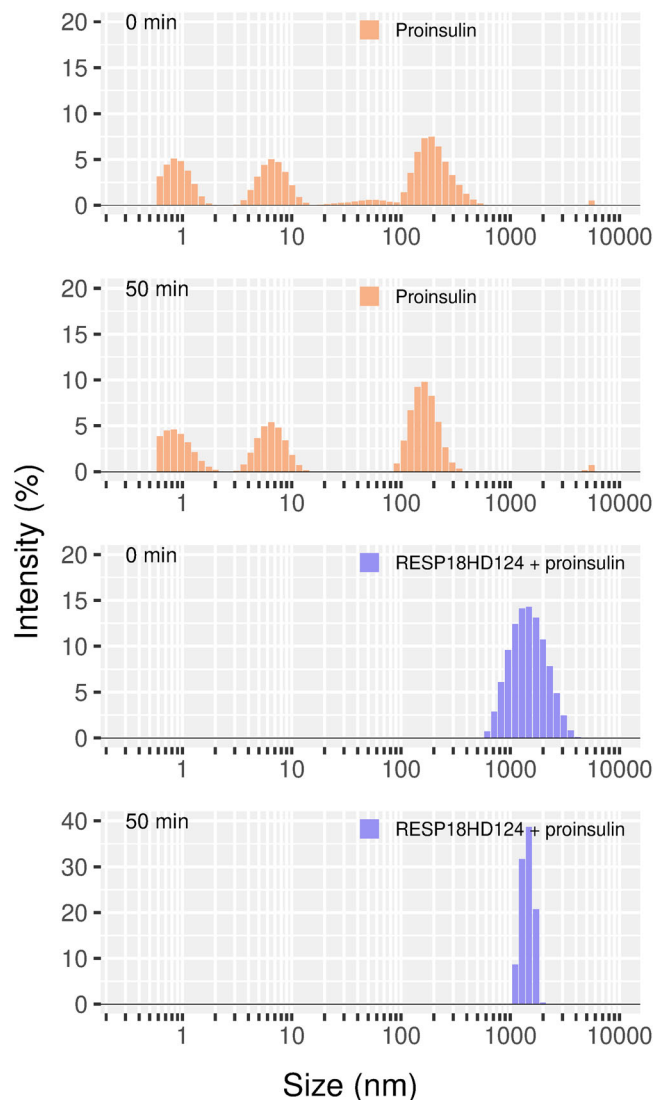
**FIGURE 8** DLS analysis of proinsulin and RESP18HD124 + proinsulin. Samples were incubated at pH 6.8, in the condensation assay conditions. Twelve or more replicates for each sample were automatically processed by the Zetasizer's software. Averages of two or more, independent experiments are shown. DLS, dynamic light scattering.

can be disordered in solution, namely the C-peptide residues 33–63 of proinsulin and residues 118–124 of RESP18HD124 (PDB ID: 2kqp; AF-Q16849 (Jumper et al., 2021), Figures S6 and S7). It is noteworthy that in the AlphaFold model of ICA512, residues 118–450 are mostly disordered, and therefore the potential condensation activity of this receptor might involve not only RESP18HD but most of the ICA512 N-terminal fragment (NTF) (see Figure 1). The inference from the structural models was consistent with sequence-based disorder predictions, which indicate that ICA512 NTF residues 112–173, 289–329, and 393–439 and the C-peptide residues 38–52 of proinsulin are disordered (Box S3) (Xue

et al., 2010). In addition, RESP18HD residues 112–127 are characterized as low-complexity and compositionally-biased sequences, which may have a bearing in condensation reactions (Necci et al., 2020).

It is also known that certain sequence patterns are indicative of the propensity to form condensates. We applied seven sequence-based predictive methods (see Section 4) to relate our findings to the conceptual framework of phase separation.

The first predictor, FuzDrop, is based in the high conformational entropy that many proteins exhibit upon binding, which can be predicted from the amino acid sequence (Hardenberg et al., 2020). FuzDrop identified residues 116–131 of RESP18HD as likely promoters of condensation. Interestingly, it also predicted several condensing sequences starting at residue 116 of the ICA512 NTF as strong inducers of condensation. On the other hand, proinsulin scored negative with FuzDrop.

The second predictor, GraPES (Kuechler et al., 2022), was originally developed to target stress-granule constituents, but it also showed predictive power for proteins that localize into other biological condensates. The method was parameterized using protein abundance, protein intrinsic disorder, annotated phosphorylation sites, $\pi$–$\pi$ contacts, intrinsic solubility, protein hydrophobicity, RNA interaction potential, and composition of amino acids to predict localization into biological condensates. The predictor was optimized with sequences longer than 140 residues, thus it cannot be used to analyze RESP18HD or proinsulin as such. Instead, we applied it to the analysis of the entire ICA512 NTF region, which includes the RESP18HD domain (Figure 1). The overall GraPES score indicates that ICA512 NTF has a low probability of being included in a biological condensate. However, several predicted features of ICA512 NTF are frequently associated to condensation propensity, namely, a high percentage of disordered residues, the amount of potential $\pi$–$\pi$ contacts, a high potential of RNA interaction, and a high percentage of isoleucine and phenylalanine residues.

The third predictor, PSPer, aims to identify FUS-like phase separating proteins, which contain prion-like domains, RNA-recognition motifs, and disordered, arginine rich regions (Orlando et al., 2019). PSPer classified ICA512 NTF as a non-phase-separating sequence and rejected for being too short the proinsulin sequence.

The fourth algorithm, catGRANULE (Bolognesi et al., 2016), was trained on the yeast proteome using sequence composition statistics and weighting residues by expected contribution to structural disorder, nucleic acid-binding propensity, sequence length, and the frequencies of arginine, glycine, and phenylalanine. Applied to other proteomes, it gave a distribution of condensing scores. Applied to the entire ICA512 NTF, it showed a
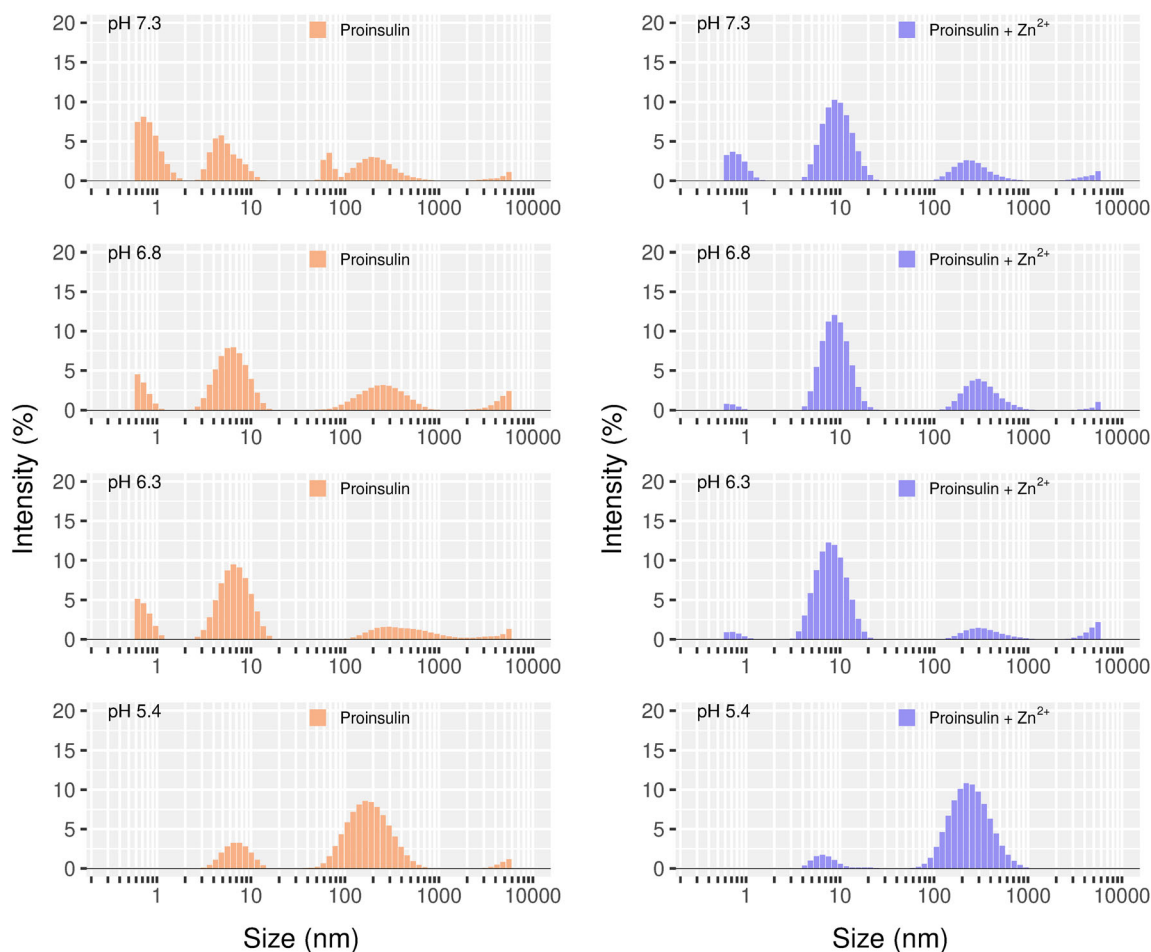
**FIGURE 9** DLS analysis of proinsulin and proinsulin–$Zn^{2+}$. Samples were incubated at the indicated pHs. Proinsulin and $Zn^{2+}$ concentrations were 20 μM and 100 μM, respectively. Twelve or more replicates for each sample were automatically processed by the Zetasizer's software. Averages of two or more, independent experiments are shown. DLS, dynamic light scattering.

propensity score that indicates granule formation propensity based on RNA binding capability and structural disordered propensities as well as amino acid patterns and polypeptide length. However, it is difficult to conclude that the RESP18HD124 section retains the condensation propensity of the whole ICA512 NTF. On the other hand, proinsulin showed a score indicative of low granule formation propensity.

The fifth predictor, PLAAC (Lancaster et al., 2014), searches protein sequences to identify probable prion subsequences using a hidden-Markov model (HMM) algorithm. Prion-like sequences have distinct features of amino acid composition such as Q/N abundance. Regarding ICA512 NTF, PLAAC predicted a prion-like subsequence spanning residues 102–143, which includes the C-terminal residues of RESP18HD. Neither RESP18HD itself nor proinsulin showed prion-like subsequences in this analysis.

The sixth predictor, DeePhase (Saar et al., 2021), was developed extracting biophysical and sequence-specific

features of phase-separating proteins, combining them with neural network-based sequence embeddings, and training machine-learning classifiers. Full-length ICA512 NTF was predicted to phase separate by DeePhase, but the RESP18HD131 subsequence and proinsulin scored negative.

The seventh method, PSPredictor (Chu et al., 2022), is a sequence-based machine learning condensate prediction tool based on data from LLPSDB (see Section 4). When applied to ICA512 NTF, PSPredictor gave a positive result, but scored negative with the RESP18HD subsequence and proinsulin.

In summary, most predictive methods identified sequence patterns indicative of condensation propensity in the ICA512 NTF, but the included RESP18HD subsequence was spotted only in two of them. The more likely explanation for this result is that the C-terminus of RESP18HD is part of a larger condensing region downstream ICA512 NTF. On the other hand, proinsulin and insulin sequences scored negative for condensation
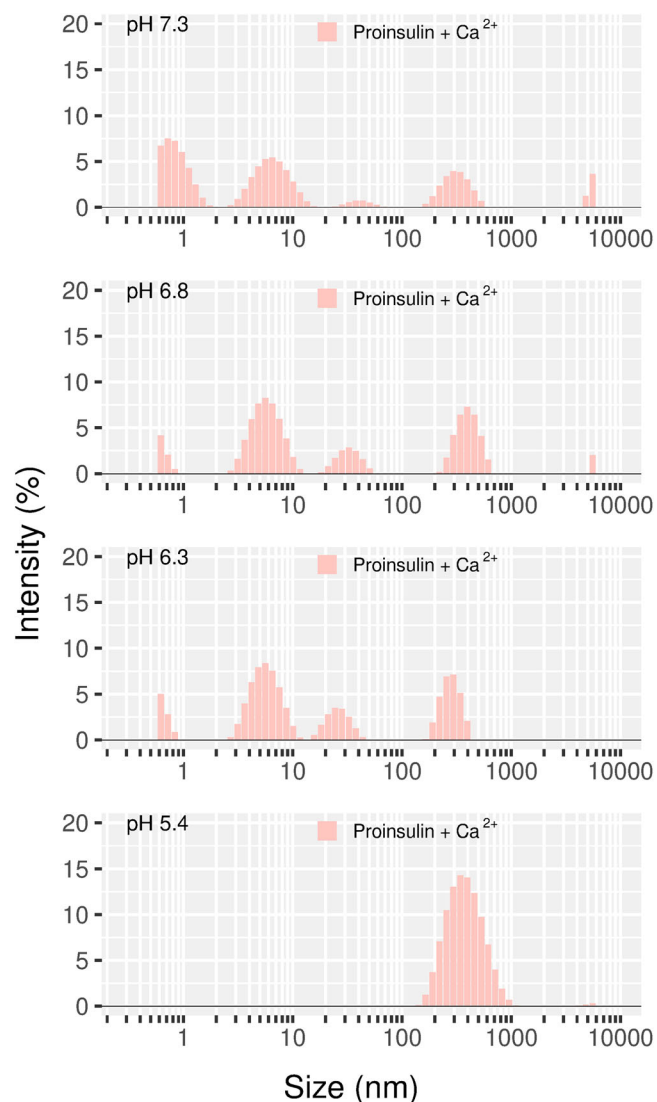
**FIGURE 10** DLS analysis of proinsulin and proinsulin–$Ca^{2+}$. Samples were incubated at the indicated pHs. Proinsulin and $Ca^{2+}$ concentrations were 20 μM and 100 μM, respectively. Twelve or more replicates for each sample were automatically processed by the Zetasizer's software. Averages of two or more, independent experiments are shown. DLS, dynamic light scattering.

propensity. Neither RESP18HD nor proinsulin exhibited sequence patterns obviously related to typical condensing proteins. However, RESP18HD did exhibit a modest enrichment in Q/N and R residues reminiscent of prion-like and RNA condensing proteins.

The computational sequence analysis and 3D model inspection indicated that residues 110–131 of RESP18HD18 are disordered. Since disorder is a strong determinant of protein condensation, we aimed to confirm that those residues are implicated in the insulin condensing reaction. To that end, synthetic peptides RESP18HD91–109, RESP18HD110–131, and scrambled RESP18HD110–131 were designed and subjected to the

condensation assay monitored by light scattering. The experiments with synthetic peptides allowed us to narrow the sequence of RESP18HD involved in condensation down to residues 91–109 MSQGLSWHDDLTQYVISQE (see Figure S8 and Box S3). Importantly, the sequence of these peptides does not contain cysteine residues, which independently confirms that the condensation reaction does not depend on the redox status of RESP18HD18 cysteine residues.

# 3 | DISCUSSION

In this work, we investigated in vitro interactions between insulin, proinsulin, and RESP18HD, potentially important for the biogenesis of SGs in cells. The first key finding was that, under conditions that mimic those along the secretory pathway, the three proteins self-associate and form nanocondensates. At the time of this investigation, the capacity of insulin to assemble and populate nanocondensates at neutral pH in vitro was well known (Dodson and Steiner, 1998; Pekar and Frank, 1972; Nielsen et al., 2001; Attri et al., 2010; Wijesekara et al., 2010; Landreh et al., 2012; Xu et al., 2012; Nilsson, 2016; Dzianová et al., 2020; Kaissaratos et al., 2021; Karmakar et al., 2022; Silva-Jr et al., 2022; Jonassen et al., 2012), but proinsulin had been much less studied in this regard (Pekar and Frank, 1972). On the other hand, in previous works, we had presented evidence of the self-condensation of RESP18HD (Sosa et al., 2016; Toledo et al., 2019). Nanocondensates are considered precursors of larger, microscopic condensates and come in a variety of material states, including liquid droplets, gels, amorphous aggregates, fibers, and semicrystalline materials (Vazquez et al., 2022). In contrast with microscopic condensates—which are sedimentable by moderate centrifugal forces and observable by conventional microscopy—nanocondensates are only detectable in light scattering experiments. This distinction is important because nanocondensates can easily go unnoticed in vivo, appearing to be fully soluble molecular assemblies.

It is also worth to mention that all the experiments in the present work were performed with untagged proteins. Although it is frequently unavoidable, the use of tags to study protein condensation can be misleading. For instance, in typical experiments, the target molecule is fused to a fluorescent tag protein, and if the fusion protein phase separates but the fluorescent tag protein does not, this is taken as evidence of condensation of the target. However, there can be several alternative explanations for such a result. A simple but important one is that—given that all proteins eventually condense under

appropriate conditions (Vazquez et al., 2022)—the increase in size brought about by the fusion can convert a non-condensing condition into a condensing one for a given target. The tag-free approach taken in this work allowed us to assess the intrinsic condensation propensity of unmodified insulin/proinsulin and RESP18HD, and thus possible artifacts due to the influence of extrinsic tags were avoided. Unless yet unidentified opposite forces are at work in vivo, the intrinsic tendency of pro/insulin and RESP18HD toward condensation should prevail during the biogenesis of SGs.

Our observation of proinsulin self-condensation provides new insights into several molecular aspects of the SG biogenesis. In the ER, after signal peptide cleavage, proinsulin folds oxidatively into its native state. At this stage, intermolecular condensation might interfere with intramolecular folding. This implies that the chaperoning machinery might counteract condensation by keeping proinsulin in a monomeric, folding-competent state (Liu et al., 2021; Liu et al., 2018; Haataja et al., 2013). In the cis-Golgi, free of the ER chaperoning system and at pH slightly below 7.0, the tendency of proinsulin to condense should prevail, resulting in dimers, hexamers, and high-order self-condensates. In the trans-Golgi, at pH slightly above 6.0, proinsulin and other protein cargoes somehow induce membrane curvature, budding, and the generation of immature granules (Nesterov et al., 2021). Initially, it was thought that sorting to immature SGs was mediated by cargo-specific receptors. However, these receptors have not been identified and the idea is being progressively abandoned. In its place, phase separation of condensed proteins has been proposed to promote nonspecifically membrane budding and therefore the assembly of immature SGs. When anchored to a budding membrane, condensed proteins may exert forces that are capable of generating a high degree of membrane curvature (Parchure et al., 2022; Nesterov et al., 2021; Day et al., 2021; Kozlov and Taraska, 2023; Schiano Lomoriello et al., 2022; Floris et al., 2022). It has also been suggested that CGB plays a central role as a condensing scaffold to recruit proinsulin and other granule cargoes as clients at the trans-Golgi step. The findings of CGB and proinsulin organized as punctate, condensate-like structures in the Golgi apparatus and of electron-dense material budding from the Golgi stack of mouse islets give support to the notion that proinsulin and CGB undergo co-condensation in this compartment (Ramazanov et al., 2021; Parchure et al., 2022). Based in our observation of in vitro spontaneous self-condensation of proinsulin, we hypothesize that, in vivo, this molecule may condense on its own and might itself be a significant driver of granule biosynthesis. In such character, proinsulin might engage into co-condensation with other granule cargoes, blurring the distinction between clients and scaffold components of the immature SG. Since the proinsulin condensation capacity is rooted in its intrinsic biophysical properties, it may condense in vivo independently of other cargo molecules, and thus explain the granulogenesis resilience to the lack of CGB (Rohli et al., 2022; Bearrows et al., 2019; Parchure et al., 2022).

A second key finding of our work was that, in vitro, proinsulin co-condenses with RESP18HD. The significance of this finding is twofold. First, since RESP18HD is a domain of the transmembrane protein ICA512, it provides a physical link between the luminal proinsulin condensate, the budding membrane, and the cytoplasm. Second, it adds ICA512 to a growing list of granular proteins that may co-condense during granulogenesis, suggesting that ICA512 RESP18HD and its protein luminal regions in overall may be part of a complex phase-separating system operating in cargo protein sorting and proteolytic processing events. The potential physical connection between the transmembrane receptor ICA512 and proinsulin nano-condensates fits well into current biophysical models in which membrane-anchored IDDs play a key control role inducing the phase separation of themselves and of other proteins on the membrane surface (Nesterov et al., 2021; Mitchison, 2020). These models are based on that the interaction with disordered proteins modulates membrane properties, the contact with condensates causes membrane remodeling, and the interaction between lipid domains and protein condensates can be reconstituted in vitro (Lee et al., 2019; Fakhree et al., 2019; Rey et al., 2020). In addition, the physical connection may be important to orchestrate the numerous processes involved in granulogenesis, particularly the recruitment of cytosolic factors involved in membrane budding and fission, and the potential ability of ICA512/IA-2 and phogrin/IA2β to modify the composition and/or accessibility of phosphoinositides (e.g., PI4P) in the membranes of the TGN and budding immature SGs. Confirmed so far, the list of proteins that may co-condense during granulogenesis includes proinsulin, insulin, CGB, and PC2, but it is likely to grow by including several others: PC1/3, CPE, CGA, VGF, phogrin, secretogranins, and amylin (Dirkx Jr and Solimena, 2012; Rohli et al., 2022; Toledo et al., 2019; Parchure et al., 2022; Rindler, 1998). What is common to these proteins is the content of IDDs, the tendency to condense, and the capacity to interact, directly or indirectly, with membranes.

A third key finding of our work regarded to the material properties of the insulin/proinsulin and RESP18HD condensates. Our DLS experiments show that in physiological-resembling conditions, that is, in the pH range of 7.3–5.4 and with or without micromolar concentrations of $Zn^{2+}$, these proteins populate molecular assemblies ranging in size from 15 to 300 nm, equivalent to $10^2$–$10^6$ molecules. These molecular condensates fall

into the definition of mesoscopic clusters or "nanocondensates," a class of condensates that is attracting growing interest for its involvement in nucleation processes such as aggregation, liquid–liquid phase separation, fibrillation, and crystallization. In this regard, nanocondensates are distinct from typical "microcondensates" which are in the realm of the micron scale (Vazquez et al., 2022).

In the ER, proinsulin has been generally envisaged as the stoichiometric association of monomers to form dimers, hexamers, or small multiple thereof. Importantly, proinsulin hexamerization is facilitated by the presence of zinc ions (Dodson and Steiner, 1998; Liu et al., 2018; Haataja et al., 2013; Kiselar et al., 2011) Our finding that, in condition mimicking the ER and with and without micromolar concentrations of $Zn^{2+}$, proinsulin populates assemblies of $10^4$–$10^5$ molecules calls for a reexamination of its folding, particularly regarding misfolding and proteostasis. According to our results, proinsulin may also populate nanocondensates in the Golgi apparatus and in immature SGs. In this regard, previous EM evidence showed the accumulation of condensed material, likely proinsulin, in the Golgi cisternae and in granules with pale cores (Parchure et al., 2022; Dzianová et al., 2020; Asai et al., 2022; Orci et al., 1987; Puri et al., 2018). At pH 5.7–5.2 and with and without micromolar concentrations of $Zn^{2+}$, the conditions prevailing during the maturation of SGs, we found that proinsulin also populates nanocondensates.

Our observation that $Zn^{2+}$ and $Ca^{2+}$ are dispensable for the formation of proinsulin nanocondensates in vitro is not in conflict with their potential role in promoting granulogesis in vivo. In guinea pig and hagfish, the proinsulin molecule lacks a histidine residue assumed essential for the coordination of zinc; however, in these species, proinsulin is normally processed, and glucose homeostasis is normal, despite the absence of insulin crystals in the mature SGs (Emdin et al., 1980). Likewise, the only $Zn^{2+}$ transporter in the beta cell, ZnT8 is only essential for normal glucose homeostasis after the prolonged environmental cell stress of a high fat diet: proinsulin conversion to insulin is normal in $ZnT8^{-/-}$ mice. Importantly, SGs in $ZnT8^{-/-}$ mice contain pale-core condensates—which confirms that $Zn^{2+}$ is essential for the formation of crystalline condensates of insulin in vivo but dispensable for condensation. Additionally, in mice isolated pancreata, no difference could be found between $ZnT8^{-/-}$ and $ZnT8^{+/+}$ in insulin release after glucose or KCl stimulation, indicating that zinc-insulin crystals do not impose a significant delay on the rate of insulin exocytosis and/or diffusion of interstitial hormone into the circulation (Lemaire et al., 2009).

Growing evidence suggests that the formation of insulin crystals does not follow the classical nucleation theory but proceeds via a two-step mechanism primed by nanocondensates. In the canonical nucleation theory crystal growth proceeds from sparse and ordered nuclei that are immersed in the solution and carry the structure of the large crystals. In the two-step mechanism, nuclei grow out of dense and disordered nanocondensates, in which the high concentration of the crystallizing molecules overcomes the high nucleation barrier and makes the process highly efficient (Kaissaratos et al., 2021). Remarkably, the nanocondensates of proinsulin that we characterized in vitro have sizes comparable to those that conform the core of a single SG (Dzianová et al., 2020; Asai et al., 2022).

Aside from size, other material properties of the condensates studied herein remain to be characterized. In principle, they could be liquid-like, gels, or solid-like. It was reported that proinsulin puncta in the Golgi apparatus displayed occasional fusion, indicating liquid-like behavior (Parchure et al., 2022). Interestingly, in concanamicyn A-treated control cells punctate proinsulin appeared diffuse, indicating the pH dependence of the material properties of the condensate. Similarly, GFP-CGB in vitro condensates were reported to have liquid-like properties and to recruit proinsulin into co-condensates (Parchure et al., 2022). On the other hand, the final products of the in vitro RESP18HD condensation and co-condensation appear to be amorphous solids (Toledo et al., 2019). Unfortunately, nanocondensates are very hard to detect in vivo, not to mention to assess their material state. Because of this, it is not clear if the scanty information available corresponds to nano or to microcondensates, and new specifically designed experiments are needed to get insight into this biophysical aspect of the biogenesis of the SG.

Finally, we note that all three proteins containing a RESP18 domain, namely ICA512, phogrin, and Resp18, are restricted in their expression to endocrine cells and neurons which share the ability to generate SGs/large dense core vesicles for the storage and regulated secretion of peptide hormones and neuropeptides, respectively. It is therefore tempting to speculate that in all these cells, RESP18 domains act in the early secretory pathway as universal pro-condensing seeds for the biogenesis of these vesicles carrying a very diverse array of cargo peptides.

# 4 | MATERIALS AND METHODS

## 4.1 | Reagents and general procedures

Chemicals were of the purest analytical grade available. Human insulin was a gift from Dr. Nestor Annibali (Denver Farma, Buenos Aires, Argentina) or purchased from Sigma (91077C). Sodium tetrathionate was

synthesized according to Schlessinger (Schlessinger, 1962). *Escherichia coli* thioredoxin (TRX) was prepared as previously described (Vazquez et al., 2015).

Reverse-phase HPLC was performed with a Water Alliance 2690 HPLC system (New Heaven, USA), a μBondapak C18 column (Waters; 150 mm length, 3.9 mm inner diameter, and particle size of 10 μm), a Waters 2487 absorbance detector, and a linear gradient of acetonitrile/water in 0.1% TFA.

## 4.2 | Dynamic light scattering

The intensity fluctuation of scattered light due to Brownian motion of particles in solution can be measured in DLS experiments, and its time evolution can be described by an intensity correlation function that is related to the hydrodynamic size of the particles. The measured diffusive relaxation rate is $\Gamma = Dq^2$, where $D$ is the diffussion coefficient and $q$ the scattering vector. $D$ is related to the particle radius, $R$, by the Stokes–Einstein equation, $D = (k_B T)/(6\pi\eta R)$, where $k_B$ is Boltzmann's constant, $T$ the temperature, $\eta$ the viscosity of the solvent, and $q$ is related to the scattering angle, $\theta$, the wavelength of light, $\lambda$, and the refractive index, $n$, by $q = n(4\pi/\lambda)\sin(\theta/2)$. DLS measurements and fitting of the correlation function were carried out with a Zetasizer Nano ZS (Malvern Instruments, Malvern, UK) (Stetefeld et al., 2016). Protein samples were illuminated by a 532 nm laser, measuring the backscattered light intensity at an angle of 175°. The accumulation time for each sample was determined automatically by the instrument software. An average of 15 measurements was used for each calculation. The inbuilt protein analysis software (Zetasizer Software 7.1) was used to calculate the size distribution of protein particles. In all measurements the temperature was controlled at 25°C and the dispersant viscosity was set to that of water (0.8872 cP) with a refractive index of 1.330. For the standard assay conditions, DLS samples were prepared either in 25 mM sodium acetate, pH 4.5, or in 100 mM HEPES, pH 6.8. Proinsulin samples were also assayed in 100 mM HEPES, pH 7.3; 100 mM HEPES, pH 6.8; 100 mM MES, pH 6.3; 100 mM sodium acetate, pH 5.4. When indicated, 100 μM ZnSO$_4$ or 100 μM Cl$_2$Ca was added to the samples.

## 4.3 | Plasmid DNA constructs and protein expression and purification

The pET9b plasmid for the expression of human ICA512 RESP18HD (residues 35–131) (UniProtKB Q16849) in *E. coli* was described previously (Toledo et al., 2019).

Truncated variants ICA512 RESP18HD90 (residues 35–90) and ICA512 RESP18HD124 (residues 35–124) were generated by inserting stop codons by site-directed mutagenesis in the original plasmid (QuikChange, Stratagene, La Jolla, CA). ICA512 RESP18HD was purified as previously described with minor modifications (Sosa et al., 2016). Briefly, refolding of purified RESP18HD124 was conducted by dialysis against 25 mM sodium acetate, pH 4.5, overnight at 4°C. The refolded protein was subjected to dialysis against oxidative buffer (25 mM sodium acetate, 5 mM 2-mercaptoethanol, 0.5 mM dithiopropionic acid, 0.5 mM cystamine, 0.5 mM cystine, pH 4.5) for 3 h at room temperature. Finally, oxidized RESP18HD124 was extensively dialyzed against 25 mM sodium acetate, pH 4.5. A similar protocol was used to purify RESP18HD90 and RESP18HD124.

Protein S-alkylation was performed using the cysteine-specific blocking-agent N-ethylmaleimide (NEM). Samples of RESP18HD124 (120 μM) were dialyzed overnight at 4°C against 100 mM potassium phosphate buffer, pH 7.2 and 6 M urea to prevent protein aggregation. The dialysate was incubated with a 10-fold molar excess NEM:SH groups for 2 h in the dark and at room temperature. Finally, the reaction was stopped by extensive dialysis against 25 mM sodium acetate buffer, pH 4.5 at 4°C. The completeness of the blocking reaction was verified by Ellman's reagent as previously described (Sosa et al., 2016).

Human proinsulin was cloned into a pET9b vector by PCR using as template the human insulin-Venus expression vector kindly provided by Dr. Susumo Seino (Kobe University, Japan). The resulting vector pET9b-hpi, was transformed into *E. coli* BL21 (DE3) cells. Transformed cells were grown in Luria Bertani medium with 50 μg/mL kanamycin. Proinsulin expression and isolation of inclusion bodies were performed as described (Sosa et al., 2016). Oxidative sulfitolysis was performed as described, with modifications (Cowley and Mackin, 1997). Briefly, proinsulin inclusion bodies were dissolved in 0.5 M Tris–HCl, 9 M urea, pH 8.6, and the reaction was initiated by the addition of sodium sulfite and fresh sodium tetrathionate at a final concentration of 0.2 M and 0.04 M, respectively. The reaction was incubated for 5 h at room temperature and stopped by the addition of glacial acetic acid. Finally, S-sulfonated proinsulin (SSO$_3$–proinsulin) was dialyzed against water and isolated as aggregated material. SSO$_3$–proinsulin aggregate was solubilized in buffer A (50 mM Tris, 8 M urea and 10 mM glycine, pH 8.6) and loaded into a Q-Sepharose Fast Flow column (2 × 5 cm, GE Healthcare). Elution was performed with a linear gradient with buffer B (50 mM Tris, 8 M urea, 10 mM glycine and 0.5 M NaCl, pH 8.6). Fractions containing SSO$_3$–proinsulin were

pooled and dialyzed against a refolding buffer (50 mM glycine, 0.5 mM EDTA and 1 M urea, pH 10.6). Oxidative refolding was performed at a protein concentration of 0.1 mg/mL with the addition of β-mercaptoethanol at a ratio of 0.75 mol per mol of cysteine S-sulfonate. The reaction was incubated under nitrogen for 16 h at 4°C with gentle agitation. Then, acid precipitation was performed in order to remove misfolded protein. Finally, oxidatively refolded proinsulin was concentrated by ultra-filtration with a Pellicon® XL Biomax 5 kDa cutoff Ultra-filtration Cassette (Merck-Millipore, MA, USA).

Proinsulin was further purified by reverse-phase HPLC chromatography (RP-HPLC) using a Delta Pak 15 µm C18 column (7.8 mm × 300 mm; Waters). Solvent A was 0.1% (v/v) TFA in water and solvent B was 80% (v/v) acetonitrile. Elution was performed with a linear gradient of 40–60% B for 40 min at a flow rate of 0.5 mL/min, and proinsulin was collected and lyophilized. The identity of the prepared proinsulin was confirmed by mass spectroscopy. Proper disulfide pairing was corroborated by V8 digestion (New England Biolabs, MA, USA) followed by HPLC analysis and mass spectrometry.

## 4.4 | Peptide synthesis and handling

Peptides P1 (RESP18HD91–109; MSQGLSWHDDLTQY-VISQE), P2 (RESP18HD110–131; MERIPRLRP-PEPRPRDRSGLAPY), and P2sc (a scrambled sequence of RESP18HD110–131; RIPMRLRPEPEPLRAPGRDRSPY) were synthesized and purified by GenScript Corporation (Piscataway, New Jersey, USA). A C-terminal tyrosine residue (underlined) was added to the corresponding RESP18HD sequences to facilitate quantitation by absorbance measurement. Peptide stock solutions were prepared from lyophilized powder in DMSO (P1) or mQ water (P2 and P2sc).

## 4.5 | Co-condensation reactions

Stock solutions of 100 µM RESP18HD in 25 mM sodium acetate, pH 4.5 were prepared afresh and filtered through a 100-nm pore filter for the assays. Stock solutions of 1.7 mM insulin or proinsulin were prepared by dissolution of the lyophilized proteins in 10 mM HCl and centrifugation at $10,000 \times g$ for 30 min at 10°C to remove residual aggregates. The basic condensation reaction protocol was carried out with 2 µM RESP18HD and 8 µM insulin/proinsulin at 20°C in 100 mM HEPES, pH 6.8. The DTT-driven condensation was carried out as in the basic protocol but with 8 µM RESP18HD, 100 µM insulin/proinsulin and 1 mM DTT.

The time course of the condensation was monitored by measuring light scattering (as apparent UV absorption at 400 nm). The aggregation state of the products of condensation reactions was analyzed by centrifugation and SDS–PAGE, and by DLS. For the SDS–PAGE analysis, the samples were spun for 5 min at 13,000 rpm in a microcentrifuge. The supernatant and pellet fractions were TCA-precipitated, and pellets were dissolved in SDS–PAGE sample buffer. Samples were heated for 5 min at 60°C in the presence of 100 mM DTT before loading into the SDS-polyacrylamide gels. For DLS analysis, the RESP18HD124 stock solutions were filtered through 100-nm-pore filters (Merck) before the assay.

## 4.6 | Sequence analysis

The propensity of full-length human ICA512 (UniProt entry Q16849) and human proinsulin (UniProt entry P01308) toward biomolecular condensation was analyzed with a battery of online servers: FuzDrop (Hardenberg et al., 2020), https://fuzdrop.bio.unipd.it/predictor; GraPES (Kuechler et al., 2022), https://grapes.msl.ubc.ca/; PSP (Orlando et al., 2019), https://bio2byte.be/b2btools/psp/; catGRANULE (Bolognesi et al., 2016), http://www.tartagialab.com/; PLAAC (Lancaster et al., 2014), http://plaac.wi.mit.edu/; DeePhase (Saar et al., 2021), https://deephase.ch.cam.ac.uk/; PSPredictor (Chu et al., 2022), http://www.pkumdl.cn:8000/PSPredictor/.

IDDs of large proteins were predicted with MobiDB-lite, an optimized method that uses eight different predictors (Necci et al., 2020) (https://mobidb.bio.unipd.it/). Otherwise, disorder of protein domains was predicted with PONDR (Xue et al., 2010) (https://www.disprot.org).

The following data banks of predicted or experimentally verified protein condensates were searched for information on insulin, proinsulin, or ICA512 sequences: LLPSDB v2.0 (Wang et al., 2022), http://bio-comp.org.cn/llpsdbv2/home.html; DrLLPS (Ning et al., 2020), http://llps.biocuckoo.cn/; FuzDB (Hatos et al., 2022), https://fuzdb.org/; PhaSepDB (Hou et al., 2022), http://db.phasep.pro/; PhaSePro (Mészáros et al., 2020), https://phasepro.elte.hu/; MLOsMetaDB (Orti et al., 2021), http://mlos.leloir.org.ar/.

### CONFLICT OF INTEREST STATEMENT
The authors declare no conflicts of interest.

### ORCID
*Mario R. Ermácora* 🔟 https://orcid.org/0000-0002-1754-4202

### REFERENCES
Andersen JN, Mortensen OH, Peters GH, Drake PG, Iversen LF, Olsen OH, et al. Structural and evolutionary relationships among protein tyrosine phosphatase domains. Mol Cell Biol. 2001;21:7117–36.

Arnaoutova I, Smith AM, Coates LC, Sharpe JC, Dhanvantari S, Snell CR, et al. The prohormone processing enzyme PC3 is a lipid raft-associated transmembrane protein. Biochemistry. 2003;42:10445–55.

Arvan P, Halban PA. Sorting ourselves out: seeking consensus on trafficking in the beta-cell. Traffic. 2004;5:53–61.

Asai S, Moravcová J, Žáková L, Selicharová I, Hadravová R, Brzozowski AM, et al. Characterization of insulin crystalline form in isolated β-cell secretory granules. Open Biol. 2022;12: 220322.

Assadi M, Sharpe JC, Snell C, Loh YP. The C-terminus of prohormone convertase 2 is sufficient and necessary for raft association and sorting to the regulated secretory pathway. Biochemistry. 2004;43:7798–807.

Attri AK, Fernández C, Minton AP. pH-dependent self-association of zinc-free insulin characterized by concentration-gradient static light scattering. Biophys Chem. 2010;148:28–33.

Bearrows SC, Bauchle CJ, Becker M, Haldeman JM, Swaminathan S, Stephens SB. Chromogranin B regulates early-stage insulin granule trafficking from the Golgi in pancreatic islet β-cells. J Cell Sci. 2019;132:jcs231373.

Blázquez M, Thiele C, Huttttner WB, Docherty K, Shennan KIJ. Involvement of the membrane lipid bilayer in sorting prohormone convertase 2 into the regulated secretory pathway. Biochem J. 2000;349:843–52.

Bolognesi B, Lorenzo Gotor N, Dhar R, Cirillo D, Baldrighi M, Tartaglia GG, et al. A concentration-dependent liquid phase separation can cause toxicity upon increased protein expression. Cell Rep. 2016;16:222–31.

Buffa L, Fuchs E, Pietropaolo M, Barr F, Solimena M. ICA69 is a novel Rab2 effector regulating ER–Golgi trafficking in insulinoma cells. Eur J Cell Biol. 2008;87:197–209.

Cao M, Mao Z, Kam C, Xiao N, Cao X, Shen C, et al. PICK1 and ICA69 control insulin granule trafficking and their deficiencies lead to impaired glucose tolerance. PLoS Biol. 2013;11: e1001541.

Carrat GR, Haythorne E, Tomas A, Haataja L, Müller A, Arvan P, et al. The type 2 diabetes gene product STARD10 is a phosphoinositide-binding protein that controls insulin secretory granule biogenesis. Mol Metab. 2020;40:101015.

Choi J-M, Holehouse AS, Pappu RV. Physical principles underlying the complex biology of intracellular phase transitions. Annu Rev Biophys. 2020;49:107–33.

Chu X, Sun T, Li Q, Xu Y, Zhang Z, Lai L, et al. Prediction of liquid–liquid phase separating proteins using machine learning. BMC Bioinform. 2022;23:1–13.

Cowley DJ, Mackin RB. Expression, purification and characterization of recombinant human proinsulin. FEBS Lett. 1997;402: 124–30.

Day KJ, Kago G, Wang L, Richter JB, Hayden CC, Lafer EM, et al. Liquid-like protein interactions catalyse assembly of endocytic vesicles. Nat Cell Biol. 2021;23:366–76.

Dikeakos JD, Reudelhuber TL. Sending proteins to dense core secretory granules: still a lot to sort out. J Cell Biol. 2007;177: 191–6.

Dirkx R Jr, Solimena M. Cholesterol-enriched membrane rafts and insulin secretion. J Diabetes Investig. 2012;3:339–46.

Dodson G, Steiner D. The role of assembly in insulin's biosynthesis. Curr Opin Struct Biol. 1998;8:189–94.

Dzianová P, Asai S, Chrudinová M, Kosinová L, Potalitsyn P, Šácha P, et al. The efficiency of insulin production and its content in insulin-expressing model β-cells correlate with their $Zn^{2+}$ levels. Open Biol. 2020;10:200137.

Emdin SO, Dodson GG, Cutfield JM, Cutfield SM. Role of zinc in insulin biosynthesis. Diabetologia. 1980;19:174–82.

Fakhree MAA, Blum C, Claessens MMAE. Shaping membranes with disordered proteins. Arch Biochem Biophys. 2019;677: 108163.

Floris E, Piras A, Pezzicoli FS, Zamparo M, Dall'Asta L, Gamba A. Phase separation and critical size in molecular sorting. Phys Rev E. 2022;106:044412.

Gehart H, Goginashvili A, Beck R, Morvan J, Erbs E, Formentini I, et al. The BAR domain protein Arfaptin-1 controls secretory granule biogenesis at the trans-Golgi network. Dev Cell. 2012; 23:756–68.

Ghahramani M, Yousefi R, Krivandin A, Muranov K, Kurganov B, Moosavi-Movahedi AA. Structural and functional characterization of D109H and R69C mutant versions of human αβ-crystallin: the biochemical pathomechanism underlying cataract and myopathy development. Int J Biol Macromol. 2020; 146:1142–60.

Haataja L, Snapp E, Wright J, Liu M, Hardy AB, Wheeler MB, et al. Proinsulin intermolecular interactions during secretory trafficking in pancreatic β cells. J Biol Chem. 2013;288:1896–906.

Hardenberg M, Horvath A, Ambrus V, Fuxreiter M, Vendruscolo M. Widespread occurrence of the droplet state of proteins in the human proteome. Proc Natl Acad Sci. 2020;117: 33254–62.

Hatos A, Monzon AM, Tosatto SCE, Piovesan D, Fuxreiter M. FuzDB: a new phase in understanding fuzzy interactions. Nucleic Acids Res. 2022;50:D509–17.

Henquin J-C, Nenquin M, Szollosi A, Kubosaki A, Notkins AL. Insulin secretion in islets from mice with a double knockout for the dense core vesicle proteins islet antigen-2 (IA-2) and IA-2β. J Endocrinol. 2008;196:573–81.

Heuck AP, Wolosiuk RA. Di-fluoresceinthiocarbamyl-insulin: a fluorescent substrate for the assay of protein disulfide oxidore-ductase activity. Anal Biochem. 1997;248:94–101.

Holmgren A. Reduction of disulfides by thioredoxin. Exceptional reactivity of insulin and suggested functions of thioredoxin in mechanism of hormone action. J Biol Chem. 1979;254: 9113–9.

Holst B, Madsen KL, Jansen AM, Jin C, Rickhag M, Lund VK, et al. PICK1 deficiency impairs secretory vesicle biogenesis and leads to growth retardation and decreased glucose tolerance. PLoS Biol. 2013;11:e1001542.

Horvath I, Wittung-Stafshede P. Cross-talk between amyloidogenic proteins in type-2 diabetes and Parkinson's disease. Proc Natl Acad Sci. 2016;113:12473–7.

Hou C, Wang X, Xie H, Chen T, Zhu P, Xu X, et al. PhaSepDB in 2022: annotating phase separation-related proteins with droplet states, co-phase separation partners and other experimental information. Nucleic Acids Res. 2022;51(D1):D460–5.

Jonassen I, Havelund S, Hoeg-Jensen T, Steensgaard DB, Wahlund P-O, Ribel U. Design of the novel protraction mechanism of insulin degludec, an ultra-long-acting basal insulin. Pharm Res. 2012;29:2104–14.

Jumper J, Evans R, Pritzel A, Green T, Figurnov M, Ronneberger O, et al. Highly accurate protein structure prediction with AlphaFold. Nature. 2021;596:583–9.

Kaissaratos M, Filobelo L, Vekilov PG. Two-step crystal nucleation is selected because of a lower surface free energy barrier. Cryst Growth Des. 2021;21:5394–402.

Kambe T, Taylor KM, Fu D. Zinc transporters and their functional integration in mammalian cells. J Biol Chem. 2021;296:100320.

Karmakar S, Ghosh T, Sankhla A, Bhattacharjee S, Katiyar V. Insulin biomolecular condensate formed in ionic microenvironment modulates the structural properties of pristine and magnetic cellulosic nanomaterials. J Mol Liq. 2022;363:119580.

Keber FC, Nguyen T, Brangwynne CP, Wühr M. Evidence for widespread cytoplasmic structuring into mesoscopic condensates. bioRxiv 2021.12.17.473234. https://doi.org/10.1101/2021.12.17. 473234

Kiselar JG, Datt M, Chance MR, Weiss MA. Structural analysis of proinsulin hexamer assembly by hydroxyl radical footprinting and computational modeling. J Biol Chem. 2011;286: 43710–6.

Kozlov MM, Taraska JW. Generation of nanoscopic membrane curvature for membrane trafficking. Nat Rev Mol Cell Biol. 2023; 24:63–78.

Kuechler ER, Jacobson M, Mayor T, Gsponer J. GraPES: the granule protein enrichment server for prediction of biological condensate constituents. Nucleic Acids Res. 2022;50:W384–91.

Kuliawat R, Arvan P. Distinct molecular mechanisms for protein sorting within immature secretory granules of pancreatic beta-cells. J Cell Biol. 1994;126:77–86.

Lancaster AK, Nutter-Upham A, Lindquist S, King OD. PLAAC: a web and command-line application to identify proteins with prion-like amino acid composition. Bioinformatics. 2014;30: 2501–2.

Landreh M, Alvelius G, Willander H, Stukenborg J-B, Söder O, Johansson J, et al. Insulin solubility transitions by pH-dependent interactions with proinsulin C-peptide. FEBS J. 2012;279:4589–97.

Lee I-H, Imanaka MY, Modahl EH, Torres-Ocampo AP. Lipid raft phase modulation by membrane-anchored proteins with inherent phase separation properties. ACS Omega. 2019;4:6551–9.

Lee S-N, Lindberg I. 7B2 prevents unfolding and aggregation of pro-hormone convertase 2. Endocrinology. 2008;149:4116–27.

Lemaire K, Ravier MA, Schraenen A, Creemers JW, Van de Plas R, Granvik M, et al. Insulin crystallization depends on zinc transporter ZnT8 expression, but is not required for normal glucose homeostasis in mice. Proc Natl Acad Sci. 2009;106:14872–7.

Li H, Wei S, Cheng K, Gounko NV, Ericksen RE, Xu A, et al. BIG3 inhibits insulin granule biogenesis and insulin secretion. EMBO Rep. 2014;15:714–22.

Lisi GP, Png CYM, Wilcox DE. Thermodynamic contributions to the stability of the insulin hexamer. Biochemistry. 2014;53: 3576–84.

Liu M, Huang Y, Xu X, Li X, Alam M, Arunagiri A, et al. Normal and defective pathways in biogenesis and maintenance of the insulin storage pool. J Clin Invest. 2021;131:e142240.

Liu M, Weiss MA, Arunagiri A, Yong J, Rege N, Sun J, et al. Biosynthesis, structure, and folding of the insulin precursor protein. Diabetes Obes Metab. 2018;20:28–50.

Mészáros B, Erdos G, Szabó B, Schád É, Tantos Á, Abukhairan R, et al. PhaSePro: the database of proteins driving liquid–liquid phase separation. Nucleic Acids Res. 2020;48:D360–7.

Mitchison TJ. Beyond Langmuir: surface-bound macromolecule condensates. Mol Biol Cell. 2020;31:2502–8.

Necci M, Piovesan D, Clementel D, Dosztányi Z, Tosatto SCE. MobiDB-lite 3.0: fast consensus annotation of intrinsic disorder flavors in proteins. Bioinformatics. 2020;36:5533–4.

Nesterov SV, Ilyinsky NS, Uversky VN. Liquid-liquid phase separation as a common organizing principle of intracellular space and biomembranes providing dynamic adaptive responses. Biochim Biophys Acta Mol Cell Res. 2021;1868:119102.

Nielsen L, Khurana R, Coats A, Frokjaer S, Brange J, Vyas S, et al. Effect of environmental factors on the kinetics of insulin fibril formation: elucidation of the molecular mechanism. Biochemistry. 2001;40:6036–46.

Nilsson MR. Insulin amyloid at injection sites of patients with diabetes. Amyloid. 2016;23:139–47.

Ning W, Guo Y, Lin S, Mei B, Wu Y, Jiang P, et al. DrLLPS: a data resource of liquid–liquid phase separation in eukaryotes. Nucleic Acids Res. 2020;48:D288–95.

Norris N, Yau B, Kebede MA. Isolation and proteomics of the insulin secretory granule. Metabolites. 2021;11:288.

Omar-Hmeadi M, Idevall-Hagren O. Insulin granule biogenesis and exocytosis. Cell Mol Life Sci. 2021;78:1957–70.

Orci L, Ravazzola M, Storch M-J, Anderson RGW, Vassalli J-D, Perrelet A. Proteolytic maturation of insulin is a post-Golgi

event which occurs in acidifying clathrin-coated secretory vesicles. Cell. 1987;49:865–8.

Orlando G, Raimondi D, Tabaro F, Codicè F, Moreau Y, Vranken WF. Computational identification of prion-like RNA-binding proteins that form liquid phase-separated condensates. Bioinformatics. 2019;35:4617–23.

Orti F, Navarro AM, Rabinovich A, Wodak SJ, Marino-Buslje C. Insight into membraneless organelles and their associated proteins: drivers, clients and regulators. Comput Struct Biotechnol J. 2021;19:3964–77.

Parchure A, Tian M, Stalder D, Boyer CK, Bearrows SC, Rohli KE, et al. Liquid–liquid phase separation facilitates the biogenesis of secretory storage granules. J Cell Biol. 2022;221:e202206132.

Paroutis P, Touret N, Grinstein S. The pH of the secretory pathway: measurement, determinants, and regulation. Phys Ther. 2004; 19:207–15.

Pekar AH, Frank BH. Conformation of proinsulin. A comparison of insulin and proinsulin self-association at neutral pH. Biochemistry. 1972;11:4013–6.

Puri S, Roy N, Russ HA, Leonhardt L, French EK, Roy R, et al. Replication confers β cell immaturity. Nat Commun. 2018;9:485.

Ramazanov BR, Tran ML, von Blume J. Sending out molecules from the TGN. Curr Opin Cell Biol. 2021;71:55–62.

Rey T, Zaganelli S, Cuillery E, Vartholomaiou E, Croisier M, Martinou J-C, et al. Mitochondrial RNA granules are fluid condensates positioned by membrane dynamics. Nat Cell Biol. 2020;22:1180–6.

Rindler MJ. Carboxypeptidase E, a peripheral membrane protein implicated in the targeting of hormones to secretory granules, co-aggregates with granule content proteins at acidic pH. J Biol Chem. 1998;273:31180–5.

Rohli KE, Boyer CK, Blom SE, Stephens SB. Nutrient regulation of pancreatic islet β-cell secretory capacity and insulin production. Biomolecules. 2022;12:335.

Saar KL, Morgunov AS, Qi R, Arter WE, Krainer G, Lee AA, et al. Learning the molecular grammar of protein condensates from sequence determinants and embeddings. Proc Natl Acad Sci. 2021;118:e2019053118.

Schiano Lomoriello I, Sigismund S, Day KJ. Biophysics of endocytic vesicle formation: a focus on liquid–liquid phase separation. Curr Opin Cell Biol. 2022;75:102068.

Schlessinger GG. Inorganic laboratory preparations. New York: Chemical Publishing Company; 1962.

Silva-Jr H, Araújo TS, da Silva AM, Scapin SM, Lima LMT. Formation of subvisible particles in commercial insulin formulations. Colloids Surf B Biointerfaces. 2022;216:112566.

Simunovic M, Evergren E, Callan-Jones A, Bassereau P. Curving cells inside and out: roles of BAR domain proteins in membrane shaping and its cellular implications. Annu Rev Cell Dev Biol. 2019;35:111–29.

Solimena M, Dirkx RJ, Hermel JM, Pleasic-Williams S, Shapiro JA, Caron L, et al. ICA 512, an autoantigen of type I diabetes, is an intrinsic membrane protein of neurosecretory granules. EMBO J. 1996;15:2102–14.

Sosa L, Torkko JM, Primo ME, Llovera RE, Toledo PL, Rios AS, et al. Biochemical, biophysical, and functional properties of ICA512/IA-2 RESP18 homology domain. Biochim Biophys Acta Proteins Proteom. 2016;1864:511–22.

Stephens SB, Edwards RJ, Sadahiro M, Lin W-J, Jiang C, Salton SR, et al. The prohormone VGF regulates β cell function via insulin secretory granule biogenesis. Cell Rep. 2017;20:2480–9.

Stetefeld J, McKenna SA, Patel TR. Dynamic light scattering: a practical guide and applications in biomedical sciences. Biophys Rev. 2016;8:409–27.

Suckale J, Solimena M. The insulin secretory granule as a signaling hub. Trends Endocrinol Metab. 2010;21:599–609.

Thor F, Gautschi M, Geiger R, Helenius A. Bulk flow revisited: transport of a soluble protein in the secretory pathway. Traffic. 2009;10:1819–30.

Toledo PL, Torkko JM, Müller A, Wegbrod C, Sönmez A, Solimena M, et al. ICA512 RESP18 homology domain is a protein-condensing factor and insulin fibrillation inhibitor. J Biol Chem. 2019;294:8564–76.

Torkko JM, Primo ME, Dirkx R, Friedrich A, Viehrig A, Vergari E, et al. Stability of proICA512/IA-2 and its targeting to insulin secretory granules require β4-sheet-mediated dimerization of its ectodomain in the endoplasmic reticulum. Mol Cell Biol. 2015;35:914–27.

Vasiljević J, Torkko JM, Knoch K-P, Solimena M. The making of insulin in health and disease. Diabetologia. 2020;63:1981–9.

Vazquez DS, Sánchez IE, Garrote A, Sica MP, Santos J. The E. coli thioredoxin folding mechanism: the key role of the C-terminal helix. Biochim Biophys Acta Proteins Proteom. 2015;1854: 127–37.

Vazquez DS, Toledo PL, Gianotti AR, Ermácora MR. Protein conformation and biomolecular condensates. Curr Res Struct Biol. 2022;4:285–307.

Wang X, Zhou X, Yan Q, Liao S, Tang W, Xu P, et al. LLPSDB v2.0: an updated database of proteins undergoing liquid–liquid phase separation in vitro. Bioinformatics. 2022;38:2010–4.

Wasmeier C, Hutton JC. Molecular cloning of phogrin, a protein-tyrosine phosphatase homologue localized to insulin secretory granule membranes. J Biol Chem. 1996;271:18161–70.

Wijesekara N, Dai FF, Hardy AB, Giglou PR, Bhattacharjee A, Koshkin V, et al. Beta cell-specific Znt8 deletion in mice causes marked defects in insulin processing, crystallisation and secretion. Diabetologia. 2010;53:1656–68.

Xu Y, Yan Y, Seeman D, Sun L, Dubin PL. Multimerization and aggregation of native-state insulin: effect of zinc. Langmuir. 2012;28:579–86.

Xue B, Dunbrack RL, Williams RW, Dunker AK, Uversky VN. PONDR-FIT: a meta-predictor of intrinsically disordered amino acids. Biochim Biophys Acta Proteins Proteom. 2010;1804:996–1010.

Yokochi Y, Sugiura K, Takemura K, Yoshida K, Hara S, Wakabayashi K-I, et al. Impact of key residues within chloroplast thioredoxin-f on recognition for reduction and oxidation of target proteins. J Biol Chem. 2019;294:17437–50.

Zhang C-F, Dhanvantari S, Lou H, Loh YP. Sorting of carboxypeptidase E to the regulated secretory pathway requires interaction of its transmembrane domain with lipid rafts. Biochem J. 2003; 369:453–60.

Zhang G, Hirai H, Cai T, Miura J, Yu P, Huang H, et al. RESP18, a homolog of the luminal domain IA-2, is found in dense core vesicles in pancreatic islet cells and is induced by high glucose. J Endocrinol. 2007;195:313–21.

Zhao H-L, Sui Y, Guan J, He L, Gu X-M, Wong HK, et al. Amyloid oligomers in diabetic and nondiabetic human pancreas. Transl Res. 2009;153:24–32.

## SUPPORTING INFORMATION

Additional supporting information can be found online in the Supporting Information section at the end of this article.